



# Magnetic and silver nanoparticle functionalized calcium carbonate particles —Dual functionality of versatile, movable delivery carriers which can surface-enhance Raman signals

Cite as: J. Appl. Phys. **126**, 203102 (2019); <https://doi.org/10.1063/1.5111973>

Submitted: 27 July 2019 . Accepted: 29 October 2019 . Published Online: 25 November 2019

Bogdan V. Parakhonskiy , Anatolii Abalymov , Anna Ivanova , Dmitry Khalek, and Andre G. Skirtach 

## COLLECTIONS

Paper published as part of the special topic on [Magnetic and Plasmonic Nanoparticles for Biomedical Devices](#)

Note: This paper is part of the Special Topic on Magnetic and Plasmonic Nanoparticles for Biomedical Devices.

 This paper was selected as an Editor's Pick



View Online



Export Citation



CrossMark

## ARTICLES YOU MAY BE INTERESTED IN

[X-ray diffraction and Raman characterization of  \$\beta\$ -Ga<sub>2</sub>O<sub>3</sub> single crystal grown by edge-defined film-fed growth method](#)

Journal of Applied Physics **126**, 205106 (2019); <https://doi.org/10.1063/1.5129226>

[Understanding leakage currents through Al<sub>2</sub>O<sub>3</sub> on SrTiO<sub>3</sub>](#)

Journal of Applied Physics **126**, 185301 (2019); <https://doi.org/10.1063/1.5119703>

[Perspective: Magnetic skyrmions—Overview of recent progress in an active research field](#)

Journal of Applied Physics **124**, 240901 (2018); <https://doi.org/10.1063/1.5048972>

Lock-in Amplifiers  
... and more, from DC to 600 MHz



# Magnetic and silver nanoparticle functionalized calcium carbonate particles—Dual functionality of versatile, movable delivery carriers which can surface-enhance Raman signals

Cite as: J. Appl. Phys. **126**, 203102 (2019); doi: [10.1063/1.5111973](https://doi.org/10.1063/1.5111973)

Submitted: 27 July 2019 · Accepted: 29 October 2019 ·

Published Online: 25 November 2019



View Online



Export Citation



CrossMark

Bogdan V. Parakhonskiy,<sup>1,a)</sup>  Anatolii Abalymov,<sup>1</sup>  Anna Ivanova,<sup>2</sup>  Dmitry Khalekchow,<sup>1</sup>  
and Andre G. Skirtach<sup>1,a)</sup> 

## AFFILIATIONS

<sup>1</sup>Department of Biotechnology, Ghent University, 9000 Ghent, Belgium

<sup>2</sup>FSRC, “Crystallography and Photonics,” RAS, 119333 Moscow, Russia

**Note:** This paper is part of the Special Topic on Magnetic and Plasmonic Nanoparticles for Biomedical Devices.

**a)Electronic addresses:** [Bogdan.Parakhonskiy@UGent.be](mailto:Bogdan.Parakhonskiy@UGent.be) and [Andre.Skirtach@UGent.be](mailto:Andre.Skirtach@UGent.be)

## ABSTRACT

Multifunctional probes play an increasing role even beyond applications in biomedicine. Multifunctionality introduced by the dual types of complementary probes is always attractive because, in this case, functionalized objects inherit the function of both materials. Porous calcium carbonate microparticles are becoming popular carriers of biomolecules and biosensors, as well as imaging enhancers. We demonstrate here a dual function of these carriers by incorporating both magnetic and silver nanoparticles. Magnetic nanoparticles enable movements and displacements by a magnetic field, while silver nanoparticles provide surface-enhanced Raman signal amplification necessary for the detection of biomolecules. Application of such dual-functional carriers is foreseen beyond the applications of biomedicine and theranostics.

Published under license by AIP Publishing. <https://doi.org/10.1063/1.5111973>

## I. INTRODUCTION

In the area of drug delivery, carriers need to be capable of releasing drugs at the desired site, avoiding drug diffusion away from the site or premature degradation. Some notable drug delivery carriers include liposomes, silica, polymeric particles, carbon-based carriers, inorganic particles such as calcium carbonate, etc. Liposomes can facilitate fusion with the plasma membrane since they have a phospholipid bilayer allowing them to fuse with cells and provide efficient drug delivery. But liposomes have some disadvantages, for example, sterilization due to sensitivity to heat. The physicochemical properties of these carriers are also rather unstable since hydrolysis of the ester bond could occur, and drugs can escape due to aggregations of liposomes.<sup>1,2</sup> Also, manufacturing liposomes is challenging since the development of multifunctional liposomes because of challenges with a coating of the surface and addition ligands, which is rather sophisticated. Besides, different liposomal formulations can affect their

biocompatibility, toxicology, and distribution. Other challenges include the storage time and chemical stability—this increases the production costs of these carriers.<sup>3</sup> Porous silica-based carriers are versatile vehicles, which have several beneficial characteristics such as biodegradability and a high surface area. Also, the porosity of the material provides possibilities for encapsulated molecules to occupy a large network of pores. One of the disadvantages of silica-based carriers is potential hemolysis of red blood cells due to the interaction with phospholipids. Another disadvantage is that porous silica NPs can induce metabolic changes leading to melanoma promotion.<sup>4</sup> In this regard, calcium carbonate represents an attractive alternative.

Calcium carbonate exists in three anhydrous crystalline forms: vaterite, calcite, and aragonite.<sup>5</sup> The most stable form is calcite, while the least stable form is vaterite.<sup>6,7</sup> Although vaterite is thermodynamically unstable due to its high solubility in water, maintaining the stability of this form can be kept through stabilization with metal ions or organic matter. Polycrystalline vaterite spheres

are attractive as nanocarriers since they have a high surface area to volume ratio and a high loading capacity due to their porous nature.<sup>8</sup> The main interest in using vaterite particles is due to their synthesis, which is more simple and less expensive than some alternatives such as liposomes. Vaterite synthesis can be done in the most cost-efficient way by mixing calcium and carbonate salts for precipitation under vigorous stirring. Its form can be controlled by stable modifications such as high supersaturation, alkaline pH, and ambient temperature.<sup>9</sup> The synthesis of multifunctional vaterite particles is simplified since different easy substance loading methods can be used, such as adsorption and coprecipitation. The particles' size in the range from 3 to 20  $\mu\text{m}$  can be tuned by adjusting the molarity and reaction time of  $\text{CaCl}_2$  and  $\text{Na}_2\text{CO}_3$  reaction mixture.<sup>10</sup> The fabrication of vaterite carriers was only recently successful as submicrometer-sized since ethylene glycol can be added to control the diffusion of the ions as well as decreasing the crystal growth rate.<sup>9,11</sup> Other methods like titration<sup>12</sup> or ultrasound agitation<sup>13</sup> allow us to obtain industrial friendly approached anisotropic vaterite particles or particles in micrometer size with the highest reaction yield. However, the synthesis of nanocarriers still remains challenging. The most frequently used size of these particles was about 4  $\mu\text{m}$  with a porosity of 40%.<sup>14</sup> Either way, submicrometer-sized carriers can be applied for active coating or drug delivery since other micrometer-sized structures such as cells or tissues can be targeted.<sup>15,16</sup>

A high potential of vaterite particles has already been explored in regenerative medicine and tissue engineering. They dissolve at low pH, and this dissolution can also occur inside body fluids since it contains several acidic metabolites. As such, the degradation products,  $\text{Ca}^{2+}$  and  $\text{CO}_3^{2-}$ , can be used extracellularly since  $\text{Ca}^{2+}$  can contribute to the formation of new tissue.<sup>17,18</sup> Vaterite particles also have other applications due to their physical and chemical properties, fast synthesis, and biodegradability. For example, vaterite crystals can be incorporated in toothpaste and mouthwashes for whitening. They have also found applications in soaps, makeup, makeup removers, wipes, etc. Also, vaterite particles can be used in absorbents, buffers, colorants, anticaking agents, fillers, and emulsion stabilizers and are, therefore, used in several personal care products.<sup>9,19</sup>

Earlier, calcium carbonate particles had been used as a template for building polyelectrolyte multilayer capsules upon dissolution of the template (calcium carbonate). Various modifications of the polymeric shell were performed by various nanoparticles (NPs) including gold and magnetic nanoparticles offering a possibility of using magnetic field and laser for releasing the contents from polymeric microcapsules,<sup>20</sup> which we extend here in application to inorganic calcium carbonate particles modifying them with magnetic and a noble metal (silver) nanoparticles. There are few recent publications about the functionalization of such porous particles by magnetic nanoparticles via adsorption<sup>21</sup> and novel, recently developed freeze-drying methods.<sup>22</sup> Apart from magnetic nanoparticles, silver nanoparticles (AgNPs), gold adsorption, or their *in situ* synthesis<sup>23,24</sup> has been used to demonstrate a possibility of forming stable inorganic matrices consisting of metal nanoparticles and minerals (calcium carbonate). It should be noted that the latter calcium carbonate can be additionally stabilized with polyelectrolyte layers.<sup>21</sup> Drug delivery carriers suited for circulation

are less suitable for capturing or carrying larger loads of molecules or for the delivery of effective doses of medicine. Drug delivery carriers with multiple functions are seen to be applicable to theranostics, where they are simultaneously used for diagnostics and therapy. In this regard, fabrication of multicompartment theranostic carrier has been performed for multicompartment microcapsules.<sup>25</sup>

Multifunctionality can also be achieved by functionalizing the carriers by different nanoparticles. The functionalization of the carrier with magnetic nanoparticles (NPs) provides the controllable motion of the carrier in magnetic fields in cells and tissues,<sup>26</sup> as well as in the living body.<sup>27</sup>

Iron oxides, which include a number of forms including magnetite ( $\text{Fe}_3\text{O}_4$ ), maghemite ( $\gamma\text{-Fe}_2\text{O}_3$ ) and hematite ( $\alpha\text{-Fe}_2\text{O}_3$ ), have traditionally been one of the most used materials due to the prevalence, cost, and practicality.<sup>28,29</sup> Several studies exist about the preparation of stable, size, and shape-controlled magnetic NPs including coprecipitation, microemulsion, thermal decomposition, solvothermal, sonochemical, microwave-assisted, chemical vapor deposition, combustion synthesis, carbon arc, and laser pyrolysis synthesis.<sup>30</sup> Functionalization of the surface of iron oxide NPs with organic molecules is carried out to preserve the colloidal stability of the particles. Biocompatible, stabilizing molecules such as citric acid are used for surface functionalization to preserve morphology and magnetic properties of NPs.<sup>31</sup> This small molecule chemisorbs to the surface of NPs and lowers the tendency of the magnetic particles to aggregate.<sup>32,33</sup> The size must allow sufficient time for the circulation of the particles after injection to reach their target organs and tissues.<sup>30</sup>

Other types of particles can be used for modification of vaterite particles. Silver NPs have been used due to their unique thermal, optical, and electrical properties. In diagnostics, silver NPs are used in biosensors, and they also possess antibacterial properties—a factor, which led to their incorporation in textile, cosmetics, and wound dressings. Also, silver NPs possess high thermal and electrical conductivity and efficiently absorb and scatter light. The latter property is dependent on the diameter and shape, where a strong interaction exists for a specific wavelength. This is referred to as the surface plasmon resonance (SPR), and it is responsible for strong scattering and absorption properties.<sup>34</sup> The surface plasmon resonance properties change due to the aggregation of NPs, thus shifting the SPR to lower energies or higher (longer) wavelengths.<sup>35</sup> The above described properties make silver NPs attractive candidates for biosensors, including surface-enhanced Raman scattering (SERS).<sup>36</sup> Both magnetic and silver NPs can be further adsorbed on diverse drug delivery carriers adding complementary functionalities. Silver on magnetic nanoparticles has been previously used by Kneipp and co-authors for separation of analyte molecules for SERS (surface-enhanced Raman scattering) detection.<sup>37</sup> SERS amplification can be extremely strong,<sup>38</sup> while platforms<sup>39</sup> have been broadly used for the detection of molecules, including pathogen detection.<sup>40</sup> It should also be noted that elaborate novel platforms are now under development, including optical waveguides for more stable SERS detection.<sup>41</sup>

In this study, porous calcium carbonate particles in the form of vaterite are designed as multifunctional carriers. The multifunctionality of porous vaterite drug delivery carriers is realized by

functionalizing them with two types of nanoparticles: (a) magnetite nanoparticles for providing motion capabilities, and (b) silver nanoparticles for enhancing the detection of molecules by SERS (surface-enhanced Raman scattering). The speed of the carriers motion in a magnetic field is investigated together with measurement of the SERS signal amplification for a model molecule—Rhodamine 6G immobilized onto the carriers. Subsequently, the cell viability has been also assessed for these new carriers. This work provides demonstration of the proof-of-principle to use motion induced by magnetic field and SERS amplification obtained by a label-free Raman detection in one carrier.

## II. MATERIALS AND METHODS

### A. Materials

All the chemical reagents were bought from Sigma-Aldrich and used without further purification. Analysis of the speed of the particles loaded with magnetite was done with a block magnet purchased from Supermagnete. This parallelepiped magnet is nickel-plated with a dimension of  $50.8 \times 50.8 \times 25.4$  mm (article ID SALE-046), and it is classified as an N40 magnet.

### B. Synthesis of the nanoparticles

#### 1. Synthesis of $\text{CaCO}_3$ micrometer-sized particles

Spherical  $\text{CaCO}_3$  with an average size of  $4 \mu\text{m}$  were synthesized, according to Volodkin *et al.*<sup>42</sup> Equal volumes of 2 ml sodium carbonate  $\text{Na}_2\text{CO}_3$  and calcium chloride  $\text{CaCl}_2$  of 0.3M were stirred together for 1 min at room temperature at a rotation speed of 500 rpm. The particles were separated by centrifugation at a speed of 3000 rpm for 3 min and washed with pure ethanol. This step was done three times. Finally, the micrometer-sized particles were left in the oven at  $70^\circ\text{C}$  for at least 1 h and stored in the freezer.

#### 2. Synthesis of $\text{Fe}_3\text{O}_4$ nanoparticles

The magnetic  $\text{Fe}_3\text{O}_4$  nanoparticles were prepared following the protocol of Elmore,<sup>43</sup> i.e., magnetite synthesis. At this moment, 10 ml of 0.37M  $\text{FeCl}_3$  and 10 ml of 0.20M  $\text{FeCl}_2$  were stirred for 30 min in 200 ml of 0.1M  $\text{NaOH}$  with a rotation speed of 600 rpm. Magnetite was collected by holding a magnet against the glass vessel and removing the supernatant. The nanoparticles were washed subsequently with 20 ml of 25 ml/mg citric acid. This procedure was done three times, after which the particles were kept in 40 ml water. The final concentration of magnetite was 12.7 mg/ml estimated via drying ( $70^\circ\text{C}$  overnight) and a weight of 10 ml suspension.

#### 3. Loading of $\text{Fe}_3\text{O}_4$ with $\text{CaCO}_3$ particles

The absorption of magnetite on the micrometer-sized particles was realized by resuspending a 10-mg portion of the particles with a chosen amount of magnetite in a total volume of 1 ml to achieve samples with different ratios of  $\text{Fe}_3\text{O}_4:\text{CaCO}_3$ . Ultrasound was used to avoid large aggregations of magnetite. This suspension was then shaken with a vortex mixer for 30 min and afterward stored minimally for 15 min in the freezer.

### 4. In situ synthesis of silver nanoparticles on $\text{CaCO}_3$ particles

The addition of silver nanoparticles with an average size of 30 nm on vaterite was based on the protocol described in Kamyshinsky *et al.*<sup>44</sup> The silver mirror reaction was done by mixing equal volumes of 0.5M  $\text{AgNO}_3$  and 0.5M  $\text{NH}_4\text{OH}$ . The solution becomes transparent after dropwise addition of  $\text{NH}_4\text{OH}$ . This so-called Tollens's reaction delivers the Tollens's reagent  $[\text{Ag}(\text{NH}_3)_2]\text{OH}$ . To absorb the silver NPs (nanoparticles) onto its carrier, 1.5 ml of water,  $150 \mu\text{l}$  of Tollens's reagent, and  $20 \mu\text{l}$  of 5% dextrose were added to its carrier. This solution was then shaken for 10 min. The functionalized particles were separated by centrifugation at a rotation speed of 3000 rpm for 3 min and stored in water.

### C. Physical characterization

#### 1. Scanning electron microscopy (SEM)

The size and shape of particles were characterized with the help of scanning electron microscopy (SEM).  $100 \mu\text{l}$  of distilled water was then added to obtain droplets for SEM examination. The measurement was performed with JSM-T330A from Joel at an operating voltage of 25 kV with secondary electrons. Before SEM, the particle droplets were coated with 15 nm sized gold nanoparticles (Bal-Tec SCD050 Sputter Coater).

#### 2. X-ray diffraction (XRD)

The phase structures of the different particle samples were examined by X-ray diffraction (XRD). The patterns were recorded with a Rigaku Miniflex-600 diffractometer (Rigaku Corporation, Tokyo, Japan) by using  $\text{CuK}\alpha$  ( $\lambda = 0.154$  nm) radiation source operating at 43 kV and 150 mA. The X-ray patterns were measured in the  $2\theta$  range  $5^\circ$ – $80^\circ$  at a scan speed  $2^\circ/\text{min}$ . The interpretation of the patterns was made with the database of the International Center of Diffraction Data (ICDD) PDF4+ was used.

#### 3. Raman spectroscopy

The enhancement factor of silver and magnetite on vaterite was observed by using SERS. A Raman microscope (Alpha300R+) was equipped with a 785 nm laser (Toptica, Munich, Germany) and a CCD camera (ANDOR iDUS 401 BR-DD, Belfast, Great Britain) cooled to  $-72^\circ\text{C}$ . The objective used was Nikon  $40\times/0.6$  NA.

For reference, Rhodamine 6G ( $10^{-3}\text{M}$ ) was deposited on the quartz surface. The spectra were recorded with 130 mW laser power and 1 min of acquisition time. The particles were incubated with various ( $10^{-3}\text{M}$ ,  $10^{-4}\text{M}$ , and  $10^{-5}\text{M}$ ) concentrations of Rhodamine 6G (laser power 15 mW, acquisition time 1 min).

The signal intensity of three characteristic peaks of Rhodamine 6G (1319, 1375, and  $1514 \text{ cm}^{-1}$ ) in a reference sample was compared to the signal intensity of Rhodamine 6G adsorbed on particles. The enhancement factor was calculated as follows:

$$\text{Enhancement factor} = \frac{\frac{P_{\text{SERS}} \cdot C_{\text{SERS}}}{I_{\text{SERS}}}}{\frac{P_{\text{control}} \cdot C_{\text{control}}}{I_{\text{control}}}} = \frac{P_{\text{SERS}} \cdot C_{\text{SERS}} \cdot I_{\text{control}}}{P_{\text{control}} \cdot C_{\text{control}} \cdot I_{\text{SERS}}},$$



with  $I$  being the Raman intensity,  $C$  the concentration in  $M$ , and  $P$  the power used during the measurement. The measurements were done in triplicate. Statistical analysis was performed using one-way ANOVA, where the significance was assigned with  $p$ -values  $< 0.05$ .

#### D. Loading efficiency

For the loading efficiency of  $\text{Fe}_3\text{O}_4$  and silver to be measured from particles, 10 mg of  $\text{CaCO}_3$  was weighted with the Quintix Analytical Balance  $30 \text{ g} \times 0.01 \text{ mg}$  from Sartorius. Statistics included 3 independent samples. Thus, the amount of magnetite loaded was estimated by weighting the dried magnetite-loaded  $\text{CaCO}_3$  first. Afterward to dissolve  $\text{CaCO}_3$  2 ml of 0.5M ethylenediaminetetraacetic acid (EDTA) was added; magnetite was then dried and weighed.

The amount of magnetite and silver loaded onto the carrier was calculated by drying the magnetite and silver-loaded  $\text{CaCO}_3$ . EDTA was added again, after which the magnetite and silver particles were dried and weighed.

#### E. Speed measurements

The speed of the functionalized particles was analyzed with an optical microscope (Leitz Wetzlar) with a  $20\times$  lens. The captured videos were taken by a color CCD camera from Monacor and imported in the computer program Pinnacle Studio 15. The particles were moved toward a block magnet with a working distance of 4 cm. A digital microscope was used to record a video when the particles moved toward the block magnet. The resulting video was used to calculate the speed of the particles using ImageJ. To calculate speed statistics, at least 50 single particles were measured.

#### F. Cell viability tests

The NHDF cells were plated separately in tissue culture flasks and cultivated in Dulbecco's modified Eagle medium supplemented with a 1% penicillin-streptomycin antibiotic antifungal cocktail of 2mM L-glutamine, containing 10% Fetal bovine serum (FBS), in a humidified incubator containing 10%  $\text{CO}_2$  at  $37^\circ\text{C}$ . The media were replaced every 3 days, and the cells were maintained in a humidified incubator at  $37^\circ\text{C}$  with 5%  $\text{CO}_2$ . Cell cultures with 75%–85% confluence were harvested using 0.25% trypsin and counted with a hemocytometer.

Cells were put in 96-well plates at the density described in the individual experiments. The next day, the microparticles were added at ratios of 10, 50, and 100 particles per cell to triplicate wells. A fresh medium was added to each of the 96 wells. Subsequently, the cells were incubated at  $37^\circ\text{C}$  overnight, together with the added materials. In the last step, to each well,  $10 \mu\text{l}$  of a fluorescence dye was added (AlamarBlue, Sigma-Aldrich), and the intensity was measured using a spectrophotometer. The experiment showed the capability of metabolically active cells to convert the AlamarBlue reagent into a fluorescent and colorimetric indicator (Fig. 1).

### III. RESULTS AND DISCUSSION

Particles are used in this study to explore the concept of a versatile carrier with dual functionality: detection and motion. For the

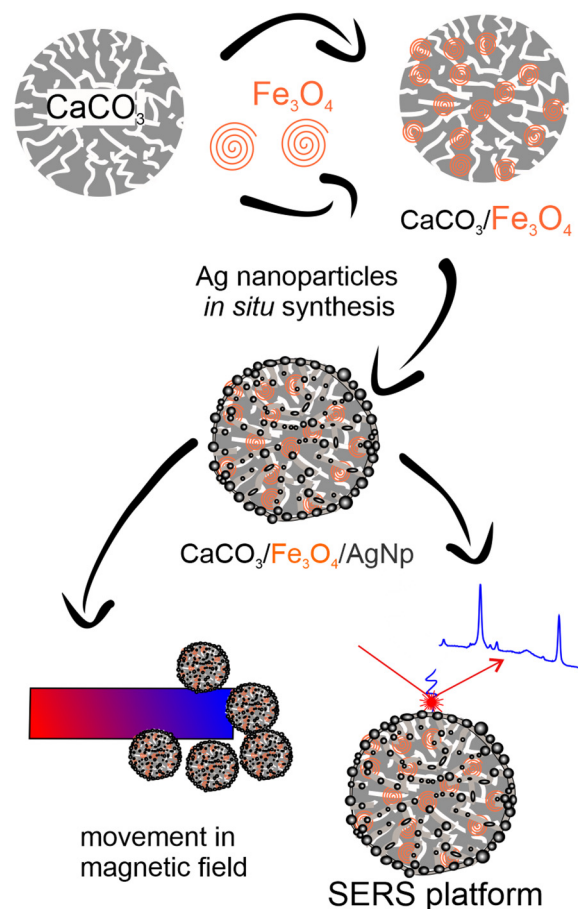


**FIG. 1.** Schematics of synthesis vaterite particles and their functionalization with magnetite particles ( $\text{Fe}_3\text{O}_4$ ) via sorption and silver nanoparticles via *in situ* synthesis (silver mirror reaction) for SERS application and movement under the magnetic field.

design of the particles which are able to move in a magnetic field and surface-enhance Raman signals, the sequential functionalization of the presynthesized porous vaterite particles with size  $\sim 3.5 \mu\text{m}$ , was performed [Scheme (1)]. The targeted delivery of drugs requires almost always a carrier. This carrier is often made out of a submicrometer or nanomatrix, where the drug of interest can be dissolved, entrapped, encapsulated, adsorbed, or attached to the surface or into the interior. The surface of the carriers can be designed in such a way as to optimize the treatment by adjusting different properties and releasing the payload, as it was already reported previously.<sup>45</sup> With this knowledge, vaterite particles were synthesized in this work via the calcium chloride and sodium carbonate precipitation methods. The average size of the particles was measured to be  $3.5 \pm 0.5 \mu\text{m}$  incurred from Figs. 2(a) and 2(d).

The following modification of vaterite particles by the adsorption of  $\text{Fe}_3\text{O}_4$  particles was performed via sorption (Sec. II). The size of the vaterite particles does not change

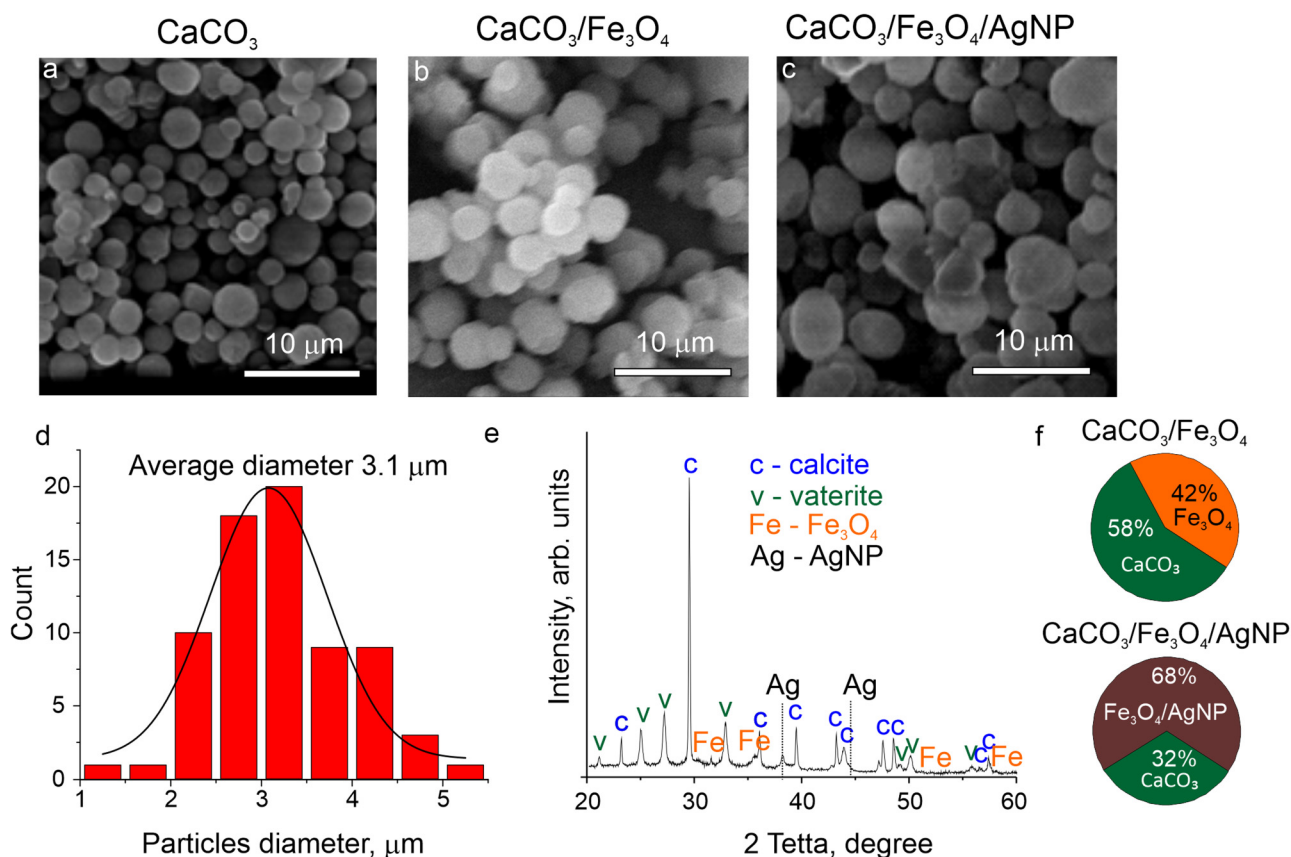
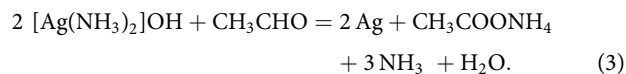
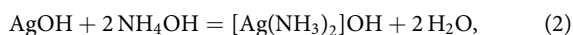


**FIG. 2.** The scanning electron microscopy image of the calcium carbonate particles (a), loaded calcium carbonate particles with Fe<sub>3</sub>O<sub>4</sub> (b), and loaded with Fe<sub>3</sub>O<sub>4</sub> and silver nanoparticles (AgNPs) (c); (d) size distribution of initial calcium carbonate particles; (e) XRD spectra of calcium carbonate particles functionalized with Fe<sub>3</sub>O<sub>4</sub> and with silver nanoparticles; (f) pie chart of the loading efficiency of the final composition of the vaterite particles loaded with Fe<sub>3</sub>O<sub>4</sub> only as well as with Fe<sub>3</sub>O<sub>4</sub> and additional silver nanoparticles.

significantly [Fig. 2(b)]. In the next step, the *in situ* synthesis of silver nanoparticles was performed. The particles used in this study are functionalized with silver NPs. Silver NPs can be synthesized by the silver mirror reaction, which leads to the creation of the Tollens's reagent [Ag(NH<sub>3</sub>)<sub>2</sub>]<sup>+</sup>. The reaction proceeds in different steps summarized in the following scheme:



This method of synthesis produces positively charged silver NPs,<sup>46</sup> while their size is dependent on the temperature of the solutions.<sup>24</sup> Particles at room temperature can be smaller than 100 nm, while solutions heated up to 50 °C produce particles with sizes that

range between 200 nm and 700 nm.<sup>47</sup> Other properties that control the size are the reaction time and the addition of surfactants. Longer reaction time and a higher concentration of the surfactants led to an increase in size.<sup>46,48</sup> The dimensions of the silver NPs in this study are restricted to the pores of the vaterite carriers, which are in the range of 20–60 nm.<sup>42</sup> Silver NPs can thus *in situ* start their nucleation in the pores of calcium carbonate particles [Fig. 2(c)].

The reaction time also affects the amount of silver NPs finally absorbed onto the vaterite carriers. For example, not all the pores will be filled after a reaction time of 10 min. However, 30 min of the reaction time causes aggregation of silver NPs on the surface of the carriers. For a reaction time of 60 min, the aggregation process extends further until the whole carrier is completely covered, similar to what was observed previously.<sup>49</sup> Functionalization with the silver particles will increase the amount of the calcite due to the recrystallization process that occurs in water (forming cubiclike particles in SEM images).

After functionalizing vaterite carriers with magnetite and silver nanoparticles, the size of vaterite particles was found to be

unaltered [Fig. 2(e)]. Furthermore, the presence of magnetite and silver can be judged from the X-ray diffraction characterization—this is confirmed by the characteristic peak at  $38.13^\circ$  and  $44.36^\circ$  for Ag and  $30^\circ$ ,  $35.45^\circ$ ,  $53.55^\circ$ , and  $57.1^\circ$  for  $\text{Fe}_3\text{O}_4$ . Both calcite and vaterite phases are seen to be present in XRD spectra, where at least 20% of the mineral was found to recrystallize to calcite. This can be assigned to the long treatment procedure during the functionalization. But most of the particles are still present in the vaterite phase as it was judged from microscopy images.

The adsorption capacity of the calcium carbonate for  $\text{Fe}_3\text{O}_4$  nanoparticles is substantially high, around 42%, as it can be seen from Fig. 2(f). But *in situ* synthesis of silver nanoparticles leads to partial desorption of magnetite and substituted with silver NPs, and the total amount was found to be 68% of the silver nanoparticles and magnetite in the final particles' composition.

Functionalization of calcium carbonate particles with magnetite is made to use the carriers for targeted delivery under a magnetic field. Therefore, subsequent tests have been done to investigate the motion of carriers in a magnetic field [Fig. 3(a)]. Specifically, subjected to a magnetic field (under the magnet of 200 kg cm), carriers moved at the speed of over 0.3 cm/s. It can also be seen from Fig. 3(a) that functionalization of carriers with additional silver nanoparticles slightly decreases the speed of the particles in a magnetic field to  $\sim 0.25$  cm/s. This can be assigned to the fact that a relative decrease of the amount of  $\text{Fe}_3\text{O}_4$  NPs as well as the additional mass of the final object reached that with silver nanoparticles.

The proposed carriers can be used for theranostics, where diagnostics and therapy are combined to identify and cure potential diseases. In laboratory conditions, no surface-modifying molecules have been added, but for real *in vivo* experiments, a number of factors need to be taken into consideration including the

adsorption of molecules on the surface of carriers. The prevention of adsorption of molecules *in vivo* can be assisted by functionalizing the carrier with PEG (polyethylene glycol). But in addition to *in vivo* circulation, the proposed particles are expected to be of interest for the separation of molecules with their subsequent identification by SERS.

Cell viability would be an important criterion of applicability of such carriers. Therefore, subsequent tests were performed to assess cell viability upon exposure and interaction of cells with vaterite carriers. The functionalization with silver and magnetite NPs does not appear to have a significant influence on the cell viability [Fig. 3(b)]. At concentrations of up to 100 particles per cell, all viability data are similar to those for the control cells.

For demonstrating the proof-of-principle for using such composite carrier particles in biosensor applications, we have chosen Rhodamine 6G molecule for loading as a model system for investigating the feasibility of its detection. We have chosen surface-enhanced Raman scattering (SERS)<sup>45,50–54</sup> as the method of detection. Hybrid materials, i.e., those combining organic and inorganic components<sup>55</sup> would be good candidates for such detection.<sup>56</sup> Raman spectra of the samples and those after the sorption on the functionalized calcium carbonate particles can be seen in Fig. 4(a). We observe typical Rhodamine peaks at  $1375\text{ cm}^{-1}$ ,  $1514\text{ cm}^{-1}$  (C-C stretching), and  $1319\text{ cm}^{-1}$  (N-H in-plane bend). Also typical C-H bend at  $1125\text{ cm}^{-1}$  and  $1180\text{ cm}^{-1}$  as well as C-C stretching at  $1650\text{ cm}^{-1}$  in-plane bent, which agrees with those reported in the literature.<sup>57</sup> For estimation of the enhancement factor of the particles, three more intense peaks were chosen [Fig. 4(a)]. Furthermore, the enhancement factor of detecting Rhodamine 6G, measured for the

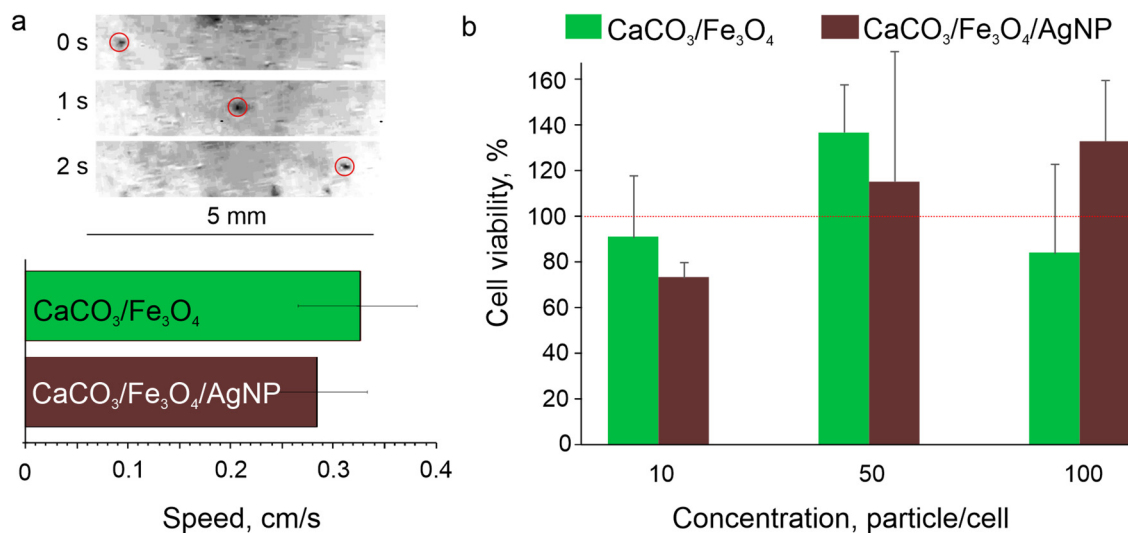


**FIG. 3.** (a) Optical images of the motion of  $\text{CaCO}_3/\text{Fe}_3\text{O}_4/\text{AgNP}$  particles and bar chart of the speed in a magnetic field for vaterite particles functionalized with  $\text{Fe}_3\text{O}_4$  with and without additional functionalization with silver nanoparticles; (b) cell viability data of vaterite particles functionalized with  $\text{Fe}_3\text{O}_4$  with and without additional functionalization with silver nanoparticles for different amount particles per cells.

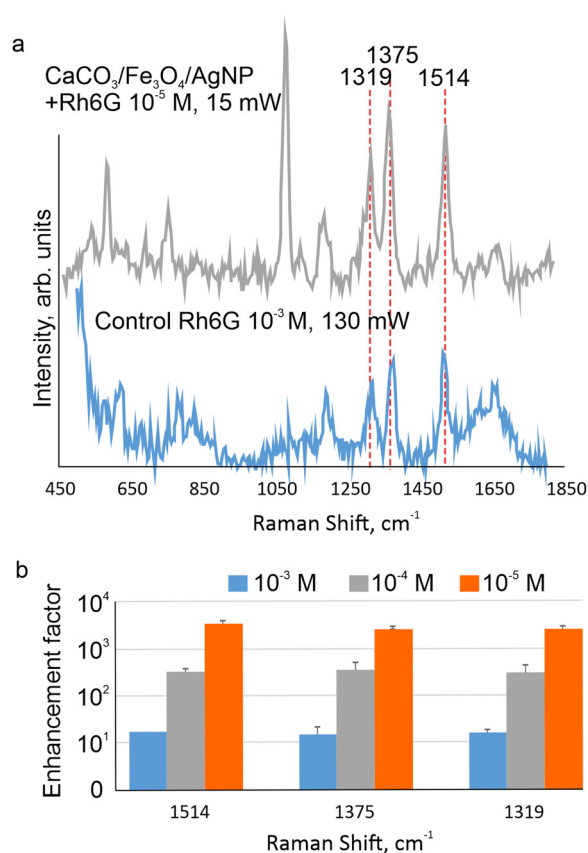


**FIG. 4.** (a) Raman spectra of Rhodamine 6G at  $10^{-3}$  M concentration probed by a laser operating at 785 nm (130 mW); and (b) SERS spectra of the Rhodamine 6G (concentrations up to  $10^{-5}$  M) adsorbed onto calcium carbonate particles functionalized with magnetic and silver nanoparticles (laser power of 15 mW).

concentrations of Rhodamine in the range of  $10^{-5}$  to  $10^{-3}$  M, was found to be up to  $10^4$  for all three peaks [Fig. 4(b)].

#### IV. CONCLUSIONS

In this work, a novel drug delivery system based on porous vaterite particles is designed possessing dual functionality and, therefore, relevant for theranostics. The proof-of-principle of such a multifunctional carrier is shown for loading various molecules, performing movements in a magnetic field, and possessing sensor capabilities. The composition of the carriers has been investigated by X-ray diffraction measurements, while their morphology has been assessed by scanning electron microscopy. The speed of motion of carriers in a magnetic field has been measured and is found to be in a range of 0.25–0.3 cm/s, while the SERS enhancement factor on these hybrid carriers is up to  $10^4$ . Cell viability studies have been performed on fibroblasts revealing that developed carriers do not possess toxicity to cells compared to control samples. Dual functionality, responsiveness to the magnetic field, and laser-induced

detection of biomolecules using the SERS effect make the designed carrier an interesting candidate for delivery of molecules and detection of molecules very relevant for the area of theranostics<sup>25</sup> responsive to multiple stimuli.<sup>58</sup> We note that in addition to drug delivery, calcium carbonate particles described in this work can be used for molecule adsorption, detection, and separation.

#### ACKNOWLEDGMENTS

We acknowledge the support from the Special Research Fund (BOF) of Ghent University (No. BOF16/FJD/029). A.A. acknowledges the Russian government funding program “Global Education.” B.V.P. acknowledges FWO (No. 1524618N) for support. A.G.S. acknowledges the support of the Special Research Fund (BOF) of Ghent University (Nos. 01IO3618, BAS094-18, and BOF14/IOP/003) and FWO-Vlaanderen (Nos. G043219 and G0D7115N). B.V.P. is an FWO postdoctoral fellow. We thank R. Kong and L. Van der Meeren for general assistance. X-ray measurement was performed using the equipment of the Shared Research Center FSRC “Crystallography and Photonics” RAS and was supported by the Russian Ministry of Education and Science (project RFMEFI62119X0035).

#### REFERENCES

- <sup>1</sup>L. Sercombe, T. Veerati, F. Moheimani, S. Y. Wu, A. K. Sood, and S. Hua, “Advances and challenges of liposome assisted drug delivery,” *Front. Pharmacol.* **6**, 286 (2015).
- <sup>2</sup>I. M. Laura, F. Dosio, and L. Cattel, “Stealth liposomes: Review of the basic science, rationale and clinical applications, existing and potential,” *Int. J. Nanomedicine* **1**, 297 (2015).
- <sup>3</sup>L. D. Danilo, *Preparation of Liposomes* (Avanti Polar Lipids, 2015).
- <sup>4</sup>C. Bharti, U. Nagaich, A. Pal, and N. Gulati, “Mesoporous silica nanoparticles in target drug delivery system: A review,” *Int. J. Pharm. Investig.* **5**, 124–133 (2015).
- <sup>5</sup>R. Rothon and C. DeArmitt, “Fillers (including fiber reinforcements),” in *Brydson's Plastics Materials*, 8th ed., edited by M. Gilbert (Butterworth-Heinemann, 2017), Chap. 8, pp. 169–204.
- <sup>6</sup>S. P. Gopi, V. Subramanian, and K. Palanisamy, “Aragonite-calcite-vaterite: A temperature influenced sequential polymorphic transformation of CaCO<sub>3</sub> in the presence of DTPA,” *Mater. Res. Bull.* **48**, 1906–1912 (2013).
- <sup>7</sup>J. D. Rodriguez-Blanco, S. Shaw, and L. G. Benning, “The kinetics and mechanisms of amorphous calcium carbonate (ACC) crystallization to calcite, via vaterite,” *Nanoscale* **3**(1), 265–271 (2011).
- <sup>8</sup>B. V. Parakhonskiy, A. M. Yashchenok, S. Donatan, D. V. Volodkin, F. Tassarolo, R. Antolini, H. Möhwald, and A. G. Skirtach, “Macromolecule loading into spherical, elliptical, star-like and cubic calcium carbonate carriers,” *Chem. Phys. Chem.* **15**, 2817–2822 (2014).
- <sup>9</sup>D. B. Trushina, T. V. Bukreeva, M. V. Kovalchuk, and M. N. Antipina, “CaCO<sub>3</sub> vaterite microparticles for biomedical and personal care applications,” *Mater. Sci. Eng. C* **45**, 644–658 (2014).
- <sup>10</sup>S. Schmidt and D. V. Volodkin, “Microparticulate biomolecules by mild CaCO<sub>3</sub> templating,” *J. Mater. Chem. B* **1**, 1210 (2013).
- <sup>11</sup>J.-P. Andreassen, “Formation mechanism and morphology in precipitation of vaterite-nano-aggregation or crystal growth,” *J. Cryst. Growth* **274**, 256–264 (2005).
- <sup>12</sup>Y. I. Svenskaya, H. Fattah, O. A. Inozemtseva, A. G. Ivanova, S. N. Shtykov, D. A. Gorin, and B. V. Parakhonskiy, “Key parameters for size- and shape-controlled synthesis of vaterite particles,” *Cryst. Growth Des.* **18**, 331–337 (2018).



- <sup>13</sup>Y. I. Svenskaya, H. Fattah, A. M. Zakharevich, D. A. Gorin, G. B. Sukhorukov, and B. V. Parakhonskiy, "Ultrasonically assisted fabrication of vaterite submicron-sized carriers," *Adv. Powder Technol.* **27**, 618–624 (2016).
- <sup>14</sup>B. V. Parakhonskiy, A. Haase, and R. Antolini, "Sub-micrometer vaterite containers: Synthesis, substance loading, and release," *Angew. Chem. Int. Ed.* **51**, 1195–1197 (2012).
- <sup>15</sup>A. A. Abalymov, R. A. Verkhovskii, M. V. Novoselova, B. V. Parakhonskiy, D. A. Gorin, A. M. Yashchenok, and G. B. Sukhorukov, "Live-cell imaging by confocal Raman and fluorescence microscopy recognizes the crystal structure of calcium carbonate particles in HeLa cells," *Biotechnol. J.* **13**, 1800071 (2018).
- <sup>16</sup>Y. I. Svenskaya, B. V. Parakhonskiy, A. Haase, V. Atkin, E. Lukyanets, D. A. Gorin, and R. Antolini, "Anticancer drug delivery system based on calcium carbonate particles loaded with a photosensitizer," *Biophys. Chem.* **182**, 11–15 (2013).
- <sup>17</sup>C. Muderrisoglu, M. S. Saveleva, A. A. Abalymov, L. Van der Meeren, A. Ivanova, V. Atkin, B. V. Parakhonskiy, and A. G. Skirtach, "Nanostructured biointerfaces based on bioceramic calcium carbonate/hydrogel coatings on titanium with an active enzyme for stimulating osteoblasts growth," *Adv. Mater. Interfaces* **5**, 1800452 (2018).
- <sup>18</sup>M. S. Saveleva, A. N. Ivanov, M. O. Kurtukova, V. S. Atkin, A. G. Ivanova, G. P. Lyubun, A. V. Martuyukova, E. I. Cherevko, A. K. Sargsyan, A. S. Fedonnikov, I. A. Norkin, A. G. Skirtach, D. A. Gorin, and B. V. Parakhonskiy, "Hybrid PCL/CaCO<sub>3</sub> scaffolds with capabilities of carrying biologically active molecules: Synthesis, loading and in vivo applications," *Mater. Sci. Eng. C* **85**, 57–67 (2018).
- <sup>19</sup>Y. Won, H. S. Jang, D.-W. Chung, and L. A. Stanciu, "Multifunctional calcium carbonate microparticles: Synthesis and biological applications," *J. Mater. Chem.* **20**, 7728 (2010).
- <sup>20</sup>D. A. Gorin, S. A. Portnov, O. A. Inozemtseva, Z. Luklinska, A. M. Yashchenok, A. M. Pavlov, A. G. Skirtach, H. Möhwald, and G. B. Sukhorukov, "Magnetic/gold nanoparticle functionalized biocompatible microcapsules with sensitivity to laser irradiation," *Phys. Chem. Chem. Phys.* **10**, 6899–6905 (2008).
- <sup>21</sup>A. Sergeeva, R. Sergeev, E. Lengert, A. Zakharevich, B. V. Parakhonskiy, D. Gorin, S. Sergeev, and D. Volodkin, "Composite magnetite and protein containing CaCO<sub>3</sub> crystals. External manipulation and vaterite → calcite recrystallization-mediated release performance," *ACS Appl. Mater. Interfaces* **7**, 21315–21325 (2015).
- <sup>22</sup>S. V. German, M. V. Novoselova, D. N. Bratashov, P. A. Demina, V. S. Atkin, D. V. Voronin, B. N. Khlebtsov, B. V. Parakhonskiy, G. B. Sukhorukov, and D. A. Gorin, "High-efficiency freezing-induced loading of inorganic nanoparticles and proteins into micron- and submicron-sized porous particles," *Sci. Rep.* **8**, 17763 (2018).
- <sup>23</sup>R. Kamysinskiy, I. Marchenko, B. V. Parakhonskiy, A. Yashchenok, Y. Chesnokov, A. Mikhutkin, D. Gorin, A. Vasiliev, and T. Bukreeva, "Composite materials based on Ag nanoparticles in situ synthesized on the vaterite porous matrices," *Nanotechnology* **30**, 035603 (2019).
- <sup>24</sup>B. V. Parakhonskiy, M. F. Bedard, T. V. Bukreeva, G. B. Sukhorukov, H. Möhwald, and A. G. Skirtach, "Nanoparticles on polyelectrolytes at low concentration: Controlling concentration and size," *J. Phys. Chem. C* **114**, 1996–2002 (2010).
- <sup>25</sup>R. Xiong, S. J. Soenen, K. Braeckmans, and A. G. Skirtach, "Towards theranostic multicompartiment microcapsules: In-situ diagnostics and laser-induced treatment," *Theranostics* **3**, 141–151 (2013).
- <sup>26</sup>I. V. Vidiashcheva, A. A. Abalymov, M. A. Kurochkin, O. A. Mayorova, M. V. Lomova, S. V. German, D. N. Khalkenkov, M. N. Zharkov, D. A. Gorin, A. G. Skirtach, V. V. Tuchin, and G. B. Sukhorukov, "Transfer of cells with uptaken nanocomposite, magnetite-nanoparticle functionalized capsules with electromagnetic tweezers," *Biomater. Sci.* **6**, 2219–2229 (2018).
- <sup>27</sup>D. V. Voronin, O. A. Sindeeva, M. A. Kurochkin, O. Mayorova, I. V. Fedosov, O. Semyachkina-Glushkovskaya, D. A. Gorin, V. V. Tuchin, and G. B. Sukhorukov, "In vitro and in vivo visualization and trapping of fluorescent magnetic microcapsules in a bloodstream," *ACS Appl. Mater. Interfaces* **9**, 6885–6893 (2017).
- <sup>28</sup>A. Ali, H. Zafar, M. Zia, I. ul Haq, A. R. Phull, J. S. Ali, and A. Hussain, "Synthesis, characterization, applications, and challenges of iron oxide nanoparticles," *Nanotechnol. Sci. Appl.* **9**, 49–67 (2016), PMID: PMC4998023.
- <sup>29</sup>Z. R. Stephen, F. M. Kievit, and M. Zhang, "Magnetite nanoparticles for medical MR imaging," *Mater. Today* **14**, 330–338 (2012).
- <sup>30</sup>A. Akbarzadeh, M. Samiei, and S. Davaran, "Magnetic nanoparticles: Preparation, physical properties, and applications in biomedicine," *Nanoscale Res. Lett.* **7**, 1–13 (2012).
- <sup>31</sup>D. L. Tran, V. H. Le, H. L. Pham, T. M. N. Hoang, T. Q. Nguyen, T. T. Luong, P. T. Ha, and X. P. Nguyen, "Biomedical and environmental applications of magnetic nanoparticles," *Adv. Nat. Sci. Nanosci. Nanotechnol.* **1**, 045013 (2011).
- <sup>32</sup>M. E. De Sousa, M. B. Fernández Van Raap, P. C. Rivas, P. Mendoza Zélis, P. Girardin, G. A. Pasquevich, J. L. Alessandrini, D. Muraca, and F. H. Sánchez, "Stability and relaxation mechanisms of citric acid coated magnetite nanoparticles for magnetic hyperthermia," *J. Phys. Chem. C* **117**, 5436–5445 (2013).
- <sup>33</sup>M. Răduciu, D. E. Creangă, and A. Airinei, "Citric-acid-coated magnetite nanoparticles for biological applications," *Eur. Phys. J. E* **21**, 117–121 (2006).
- <sup>34</sup>J. J. Mock, M. Barbic, D. R. Smith, D. A. Schultz, and S. Schultz, "Shape effects in plasmon resonance of individual colloidal silver nanoparticles," *J. Chem. Phys.* **116**(15), 6755–6759 (2002).
- <sup>35</sup>S. L. Smitha, K. M. Nissamudeen, D. Philip, and K. G. Gopchandran, "Studies on surface plasmon resonance and photoluminescence of silver nanoparticles," *Spectrochim. Acta: Part A: Mol. Biomol. Spectrosc.* **71**(1), 186–190 (2008).
- <sup>36</sup>L. Gharibshahi, E. Saion, E. Gharibshahi, A. H. Shaari, and K. A. Matori, "Structural and optical properties of ag nanoparticles synthesized by thermal treatment method," *Materials* **10**, 402 (2017).
- <sup>37</sup>M. Gühlke, S. Selve, and J. Kneipp, "Magnetic separation and SERS observation of analyte molecules on bifunctional silver/iron oxide composite nanostructures," *J. Raman Spectrosc.* **43**, 1204–1207 (2012).
- <sup>38</sup>A. M. Yashchenok, A. Masic, D. A. Gorin, B. S. Shim, N. A. Kotov, P. Fratzl, H. Möhwald, and A. G. Skirtach, "Nanoengineered colloidal probes for Raman-based detection of biomolecules inside living cells," *Small* **9**, 351–356 (2013).
- <sup>39</sup>D. Graham, M. Moskovits, and Z.-Q. Tian, "SERS—Facts, figures and the future," *Chem. Soc. Rev.* **46**, 3864–3865 (2017).
- <sup>40</sup>D. Zopf, A. Pittner, A. Dathe, N. Grosse, A. Csáki, K. Arstila, J. J. Toppari, W. Schott, D. Dontsov, G. Uhlrich, W. Fritzsche, and O. Stranik, "Plasmonic nanosensor array for multiplexed DNA-based pathogen detection," *ACS Sensors* **4**, 335–343 (2019).
- <sup>41</sup>A. Raza, S. Clemmen, P. Wuytens, M. Muneeb, M. Van Daele, J. Dendooven, C. Detavernier, A. Skirtach, and R. Baets, "ALD assisted nanoplasmonic slot waveguide for on-chip enhanced Raman spectroscopy," *APL Photonics* **3**, 116105 (2018).
- <sup>42</sup>D. V. Volodkin, N. I. Larionova, and G. B. Sukhorukov, "Protein encapsulation via porous CaCO<sub>3</sub> microparticles templating," *Biomacromolecules* **5**, 1962–1972 (2004).
- <sup>43</sup>W. Elmore, "Ferromagnetic colloid for studying magnetic structures," *Phys. Rev.* **54**, 309–310 (1938).
- <sup>44</sup>R. Kamysinskiy, I. Marchenko, and B. Parakhonskiy, "The vaterite porous matrices composite materials based on Ag nanoparticles in situ synthesized on the vaterite porous matrices," *Nanotechnology* **30**, 035603 (2019).
- <sup>45</sup>K. Kneipp, H. Kneipp, and J. Kneipp, "Surface-enhanced Raman scattering in local optical fields of silver and gold nanoaggregates from single-molecule Raman spectroscopy to ultrasensitive probing in live cells single-molecule Raman scattering in local," *Acc. Chem. Res.* **39**, 443–450 (2006).
- <sup>46</sup>J. Soukupová, L. Kvítek, A. Panáček, T. Nevěčná, and R. Zbořil, "Comprehensive study on surfactant role on silver nanoparticles prepared via modified Tollens process," *Mater. Chem. Phys.* **111**, 77–81 (2008).

- <sup>47</sup>R. Dondi, W. Su, G. Griffith, G. Clark, and G. Burley, "Highly size and shape controlled synthesis of silver nanoparticles via a templated Tollens reaction," *Small* **8**, 770–776 (2012).
- <sup>48</sup>Y. Yin, Z. Zhong, B. D. Gates, Z.-Y. Li, Y. Xia, and S. Venkateswaran, "Synthesis and characterization of stable aqueous dispersions of silver nanoparticles through the Tollens process," *J. Mater. Chem.* **12**, 522–527 (2002).
- <sup>49</sup>T. V. Bukreeva, I. V. Marchenko, B. B. V. Parakhonskiy, Y. V. Grigor'ev, and Y. V. Grigor'ev, "Formation of silver nanoparticles on shells of polyelectrolyte capsules using silver-mirror reaction," *Colloid J.* **71**, 596–602 (2009).
- <sup>50</sup>K. Hering, D. Cialla, K. Ackermann, T. Dörfer, R. Möller, H. Schneidewind, R. Mattheis, W. Fritzsche, P. Rösch, and J. Popp, "SERS: A versatile tool in chemical and biochemical diagnostics," *Anal. Bioanal. Chem.* **390**, 113–124 (2008).
- <sup>51</sup>H. Ko, S. Singamaneni, and V. V. Tsukruk, "Nanostructured surfaces and assemblies as SERS media," *Small* **4**, 1576–1599 (2008).
- <sup>52</sup>C. Krafft, M. Schmitt, I. W. Schie, D. Cialla-May, C. Matthäus, T. Bocklitz, and J. Popp, "Label-free molecular imaging of biological cells and tissues by linear and nonlinear Raman spectroscopic approaches," *Angew. Chemie Int. Ed.* **56**, 4392–4430 (2017).
- <sup>53</sup>M. Tebbe, P. Cherepanov, E. V. Skorb, S. K. Poznyak, J. G. De Abajo, A. Fery, D. V. Andreeva, R. A. A. Puebla, and N. Pazos-Perez, "SERS platforms of plasmonic hydrophobic surfaces for analyte concentration: Hierarchically assembled gold nanorods on anodized aluminum," *Part. Part. Syst. Charact.* **31**, 1134–1140 (2014).
- <sup>54</sup>N. Bontempi, L. Carletti, C. De Angelis, and I. Alessandri, "Plasmon-free SERS detection of environmental CO<sub>2</sub> on TiO<sub>2</sub> surfaces," *Nanoscale* **8**, 3226–3231 (2016).
- <sup>55</sup>M. S. Saveleva, K. Eftekhari, A. Abalymov, T. E. L. Douglas, D. Volodkin, B. V. Parakhonskiy, and A. G. Skirtach, "Hierarchy of hybrid materials—The place of inorganics-in-organics in it, their composition and applications," *Front. Chem.* **7**, 1–21 (2019).
- <sup>56</sup>R. V. Chernozem, M. A. Surmeneva, V. Atkin, B. Krause, T. Baumbach, B. V. Parakhonskiy, D. Khalek, A. G. Skirtach, and R. A. Surmenev, "Plasmonic hybrid biocomposite as an effective substrate for detection of biomolecules by surface-enhanced Raman spectroscopy," *Russ. Phys. J.* **61**, 1288–1293 (2018).
- <sup>57</sup>C. Wu, E. Chen, and J. Wei, "Surface enhanced Raman spectroscopy of rhodamine 6G on agglomerates of different-sized silver truncated nanotriangles," *Colloids Surf. A* **506**, 450–456 (2016).
- <sup>58</sup>M. Delcea, H. Möhwald, and A. G. Skirtach, "Stimuli-responsive LbL capsules and nanoshells for drug delivery," *Adv. Drug Deliv. Rev.* **63**, 730–747 (2011).